Investigation on PTO Control of a Combined Axisymmetric Buoy-WEC(CAB-WEC)

Fankai Kong[1], Weiming Su[1], Hengxu Liu[2*], Maurizio Collu[4], Zi Lin[4], Hailong Chen[2], Xiongbo Zheng[3]

1 College of Mechanical and Electrical Engineering, Harbin Engineering University, Harbin 150001, China;
2 College of Shipbuilding Engineering, Harbin Engineering University, Harbin 150001, China;
3 College of Mathematics Science, Harbin Engineering University, Harbin 150001, China;
4 Department of Naval Architecture, Ocean and Marine Engineering, University of Strathclyde, Glasgow, UK G4 0LZ
* Correspondence: liuhengxu@hrbeu.edu.cn(Hengxu Liu)

Abstract: The Combined Axisymmetric Buoy (CAB), a vertical axisymmetric buoy, has the potential to deliver a high energy absorption power. Considering the CAB-Wave Energy Converters (WEC), in order to achieve higher efficiency, the Power Take Off (PTO) systems, which converts the float motion into energy output, needs to be properly controlled. In this paper, a PTO control method for a CAB-WEC under irregular wave conditions is proposed. Based on the semi-analytical solution obtained in the time domain, a numerical optimization is carried out. The optimal PTO damping coefficients under different wave conditions are obtained, by considering the parameter defined as "capture width ratio". The expression of the optimal PTO damping coefficient in the frequency domain is derived by an analytical method. Based on the semi-analytical solution of time domain dynamic characteristics and analytical method, a comparison between frequency domain optimization and time domain optimization is presented. In general, the two approaches arrive to very similar conclusions, even if with the time domain methodology a slightly higher capture width ratio is achieved. The experimental results have been used to validate the time domain optimization method and the variation in optimal average capture width ratio results.

Key words： CAB-WEC; Semi-analytical; PTO control; Numerical analysis; Experimental method

1. Introduction

Recent trends in the international sustainable energy strategy have led to a proliferation of studies on renewable energy. Of particular interest is the development of wave energy converters (WECs). A combined axisymmetric buoy (CAB) has the potential to have a higher energy absorption power. It has smaller size and less dependence on waves, so it is flexible and economical to deploy on the ocean. A key aspect of the energy absorption efficiency of the CAB is its power take off (PTO) control. The principle of the PTO control is to improve the wave energy absorption power of the energy capture device by changing the parameters of the PTO device. As one of the control methods, the optimal control of the damping coefficient of PTO device can be intuitively embodied in the mathematical model to improve the absorption power of energy capture device. By changing the damping coefficient of the PTO device, the maximum absorption power of the device can be achieved. Previous studies are limited to the energy conversion control method of the single cylinder buoy. So far, however, very little attention has been paid to the study of an optimal control method involving the PTO damping coefficient in a CAB-WEC. This paper therefore has as aim the optimization of the PTO damping coefficient on a CAB-WEC in the frequency and time domains.

The optimal control of a PTO damping coefficient originates from the hydrodynamic performance analysis of floating structures. As a popular method for calculating the hydrodynamic performance of buoys, the semi-analytical solution is a major area of interest within the field of potential flow theory. The research on analytical algorithms dates back to the work of Miles and Gilbert[1]. They have done a great quantity of research on different types of vertical cylinders, dividing the watershed into several cylindrical subdomains, and matching the eigenfunction expansion in different subdomains. Based on the research of Miles and Gilbert, Garrett[2] obtained the wave excitation forces and moments for horizontal and vertical analysis of wave action on a fixed circular dock. Yeung[3]and Sabuncu and Calisal[4]studied a free cylinder buoy on the wave surface, deducing the analytical solutions of diffraction and radiation problems. Based on these analytical studies, the analytical expressions of wave excitation force and hydrodynamic coefficients of the cylinder were generated. Mavrakos[5]studied the diffraction of a circular column with a finite thickness portiforium, and illustrated the superiority of the Galerkin method in the calculation of velocity potential boundary matching in complex multi-basins. Kokkinowrachos et al. [6] analysed the motion of a vertical axisymmetric object of revolution under waves. The arc surface of a vertical object of revolution was decomposed into a circular stepped surface, and the velocity potential expressions of each annular basin were obtained to solve the wave excitation force. Drobyshevski[7] obtained the analytical solutions of

wave forces on truncated cylindrical platforms in very shallow waters by the progressive matching method. The hydrodynamic coefficients of three degrees of freedom motions, i.e. heave, surge and pitch, were solved according to the matching conditions in the inner and outer regions. Shen et al. [8] proved that the expressions of radiation and diffraction velocity potential were correct through comparing them with the results of the boundary element method by carrying out hydrodynamic parametric studies of a cylindrical buoy. Mavrakos and Katsaounis[9] calculated the dynamic characteristics of the oscillating buoy by the semi-analytical method in terms of diffraction and radiation. The axisymmetric eigenfunction of the velocity potential was expanded into the appropriately defined annular fluid region around the object, and matched at the boundary of the adjacent fluid region by the continuity of the hydrodynamic pressure and radial velocity. Moghadaszadeh and Khaji[10] proposed a semi-analytical solution on a vertical cylinder with arbitrary cross-section in an unbounded domain. Filianoti et al. [11] compared the wave loads on a two-dimensional horizontal underwater cylinder by semi-analytical method, and experimental results. The comparison results prove the consistency of both and the correctness of the semi-analytical method. Existing research recognizes the role of potential flow theory, be it an in-house code or commercial software. Liu et al.[12] derived the semi-analytical solution for the javelin wave energy converter, by using the frequency domain characteristic function, and applied the wave force and frequency domain hydrodynamic coefficients to the impulse response function method to obtain the dynamic response and power extracted. Zheng et al.[13] derived the hydrodynamic coefficients and exciting forces of the heave modes of the wave energy device by using a coupled hydrodynamic analysis method, and also derived the heave coupled motion equation of the device. The calculation and experimental results of the heave amplitude response operator and the energy conversion efficiency of the device were compared. Guo et al.[14] used a CFD method to analyse the single-degree-of-freedom pendulum, pitching buoy and its coupled motion (without dynamic output damping), and regular wave damping oscillation. The hydrodynamic characteristics and wave energy conversion characteristics under typical wave conditions are analyzed. Lu et al.[15] presented a time domain response estimation method based on a state-space model approach, which considers the convolution term of the floating structure and improves the computational efficiency with respect to a traditional step-by-step approach. Based on the linearized potential flow theory, Xu et al.[16] carried out a numerical analysis of spherical and cylindrical point absorbers wave energy converters. The wave-structure interaction is analyzed by boundary element method, and the spheres and cylinders with the same geometric scale and submergence depth are compared. Wang and Yeung[17] proposed a simple and feasible hybrid integral equation method for calculating the frequency domain hydrodynamic characteristics of objects with vertical symmetric axes in waves. By comparing with the experimental results, it is proved that the method can accurately predict the additional heave mass and wave excitation force of coaxial cylindrical WEC. Kim et al.[18] studied the performance of hemispherical point absorption energy converter with hydraulic power output system. The displacement and wave power of a hemispherical buoy under different water pressures and input waves are calculated, and the optimum conditions for maximum wave power are determined. However, these studies are highly dependent on the discretization of the calculation domain and their numerical accuracy. Without a unified standard calculation method, it is difficult to reveal the hydrodynamic calculation's basic principles. In addition, the numerical calculation method is often time-consuming and has a high computational cost, preventing the analysis of large numbers of load cases, necessary for the optimization. Therefore, it is necessary to develop a fast and accurate semi-analytical method to calculate the hydrodynamic characteristics of PAWEC.

Based on the analysis of the hydrodynamic characteristics of the buoy, the WEC requires reasonable control according to the PTO system parameters. Early researches show that when the incident wave frequency and the natural frequency of the wave energy conversion system are close to each other, the wave energy conversion efficiency of the point-suction device achieves the optimum. All of the control theory of the early PAWEC is based on the above-mentioned theory. Latching control was proposed by Budal and Falnes[19]. Its control principle is to synchronize the motion of the buoy with the wave by reducing the natural frequency of the oscillating buoy so as to make the device in a quasi-resonant state. Unlike the latching control method, declutch control mainly works on the PTO system rather than on the oscillating buoy. Babarit and Clément[20] have made a thorough research of this control algorithm, and expatiated its effectiveness in increasing the wave energy capture width on the oscillating buoy WEC. Unlike some control methods relying on sea states, declutch control is able to be simply implemented. It just requires the addition of an auxiliary valve to the hydraulic circulation path. This method has been applied to the Searev device, and the theoretical validity of the control algorithm has been proved under regular and irregular wave conditions. Salter[21] developed a Reactive Control (RC) method for capturing instantaneous maximum wave energy through long-term continuous control of PTO systems. RC is a continuous control algorithm, which is realized by the PTO of the device itself to provide a reaction force to balance the inherent resistance (depending on elasticity, moment of inertia and damping), so that the system can maintain its optimal state when capturing energy. Salter's duck-type device adopts the above control algorithm, and the reaction force is proportional to the angular displacement and acceleration of the buoy. However, the control method is limited to regular wave conditions. Under irregular waves, the demand for predicting future wave parameters and the subsequent calculation time will

cause difficulties in real-time control of RC. Brekken[22] applied the Model Predictive Control (MPC) theory proposed by Rossiter[23] to the PAWEC. It was found that the advantages of MPC lie not only in the variety of available wave energy devices and PTO systems, but also in the consideration of the limitation of wave energy device motion speed and displacement amplitude, which can effectively improve the safety of a wave energy conversion system. Abraham and Kerrigan[24] analysed the optimal control of PAWEC energy conversion by the MPC method with constraints and the projection gradient method. They showed that the global convergence point can be achieved with a few iterations. Jin et al.[25] studied the combined effects of geometric structure and power output damping on a PAWEC wave energy converter. The power conversion performance of the device was compared by using the power output time signal with variable damping coefficient. The results show that when a suitable PTO damping is applied to the conical streamlined bottom structure device, the optimal power can be increased up to 70% under regular and irregular waves (compared with the cylindrical flat bottom device). On the basis of optimal control theory, Abdelkhalik and Zou[26] derived a control law suitable for heave wave energy converter. The numerical experiments show that in the linear WEC system, the energy harvesting level of the simple model control approaches the maximum theoretical limit predicted by the singular arc control. Na et al.[27] proposed a robust adaptive optimal control strategy for wave energy converters. The simulation results show that the method is robust to model uncertainties and greatly reduces the computational cost. Zhan et al.[28] proposed a new feedback unsteady model predictive control (MPC) strategy for WEC. This strategy can explicitly incorporate wave prediction information into MPC strategy to improve the performance of WEC control. At present, the main issues of common PTO control algorithms are: It is impossible to improve the energy absorption efficiency of the device from the essence of the energy absorption principle; the control of PTO under irregular wave conditions is more complex, and more energy is needed to control the PTO parameters, which is not conducive to the improvement of energy absorption efficiency.

In view of the shortcomings of the current hydrodynamic calculation methods, the expressions of velocity potential, additional mass, radiation damping coefficient and wave excitation force in each region of the oscillating buoy are obtained by the Eigenfunction Expansion Matching (EEM) method. The corresponding results have been validated through a comparison with commercial software. Aiming at a PTO control algorithm, this paper presents a PTO control method for WEC of a CAB under irregular waves. Based on the semi-analytical solution of time domain dynamic characteristics, the numerical optimization of a CAB is carried out. The optimal PTO damping coefficients under different wave conditions are obtained by establishing the criterion of capture width ratio. The expression of optimal PTO damping coefficient in the frequency domain is given by an Analytical method. The relationship between the optimal PTO damping coefficient in the frequency domain and time domain is obtained by comparing the linear control method with the time domain optimization method. The optimal ratio of the PTO damping coefficient to optimal average capture width in the time domain under different irregular wave conditions is analyses and verified by experiments. The time-domain control method adopted in this paper can provide an optimal control of the PTO device of WEC under irregular waves, and achieve the maximum energy capture width ratio of WEC by changing the PTO damping coefficient under different wave conditions. The expressions of the optimal PTO damping coefficient and the optimal capture width ratio of the proposed frequency domain optimization method intuitively reflect the variation of the two parameters with frequency. By comparing the results of the frequency domain optimization with those of the time domain control, the relationship between the optimal dynamic output shaft damping coefficient and the optimal capture width ratio obtained in the frequency domain and the time domain control method is obtained, and an approximate value for engineering applications is given.

2. Mathematical Formula

The PTO control system aims at deriving the optimal damping coefficients under different wave conditions in the frequency domain and time domain. Considering the hydrodynamic coefficients of CAB, the semi-analytical method based on the boundary discretization method (BDM) proposed by Zhang (2016) is applied to the axisymmetric buoy described in this paper. The semi-analytical expressions of the hydrodynamic coefficients of the buoy, such as wave force, additional mass and radiation damping, are obtained. Based on a single degree of freedom vibration assumption and a linear PTO system, the expressions of optimal PTO damping coefficient and optimal capture width ratio of CAB are obtained in the frequency domain analysis. The impulsed response function (IRF) method is used to transform the frequency domain component into the time domain component, and an irregular wave theory is used to derive the potential flow time domain solution and energy conversion efficiency of CAB motion under irregular wave.

2.1 Semi-analytical solution of the hydrodynamic coefficient of a CAB-WEC in the frequency domain by EEM method

Fig. 1(a) shows the CAB-WEC developed by Harbin Engineering University. It is a vertical axisymmetric buoy with a cylindrical body and axisymmetric surface. The maximum radius of the CAB is R and the total draft is d with the bottom water depth of h. The bottom shape of the CAB is divided into two parts: the upper half of the buoy($-t < z < 0$)is a cylinder with radius R, and the lower half ($t < z \le t+1$)is the bottom of the surface of the buoy. The bottom shape of the buoy is based on the BW (Berkeley Wedge) curve obtained in Madhi et al.[29]. The BW is a 2D shape which was designed by Madhi et al. through viscous numerical calculation and optimization at the University of California, Berkeley. It can minimize the viscous damping in heave mode to improve the power absorption. The 2D curve is rotated axis-symmetrically along the Z-axis to form a CAB which is expressed in Fig. 1(b). The 2D curve can be expressed by a fourth-order polynomial function as follows:

$$r = F(z) = 0.05926(z+1)^2 + 3.88147(z+1)^3 - 2.94074(z+1)^4 \quad (1)$$

A boundary approximation model is established as shown in Fig. 1(c). Vertical axisymmetric floats have complex boundaries, so it is impossible to find the characteristic functions satisfying the boundary conditions directly by separating variables. According to the axis-symmetry of the buoy, the boundary of the symmetrical surface is discretized into several continuous annular stepped surfaces. Then, based on the classical analytical method of the cylindrical basin, when the number of boundary discretization reaches a certain value, the eigenfunctions of several annular stepped surfaces are satisfied to approximate the boundary of the axis-symmetrical surface, and then the hydrodynamic problems of the float with complex configuration are solved.

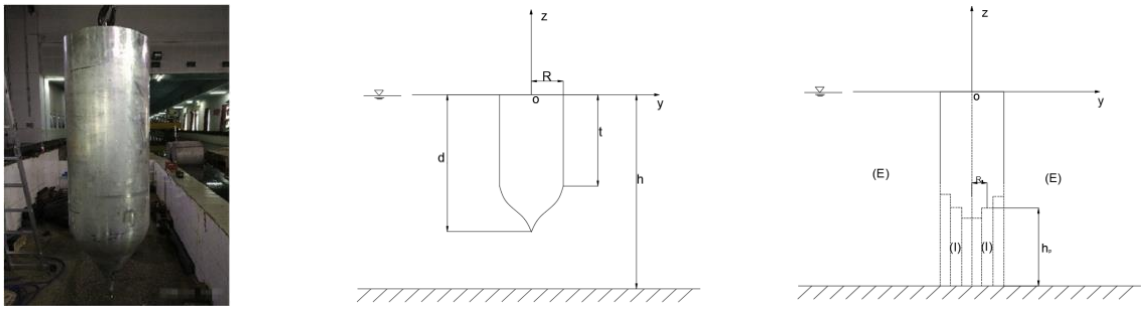

(a) The material object of the CAB (b) Geometric description of the CAB (c) The definition of fluid subdomains

Fig. 1. The material object of the CAB and the definition of fluid subdomains

According to the hypothesis of linear micro-amplitude wave, the spatial velocity potential of the flow field around the float can be decomposed into cylindrical coordinates[30].

$$\Phi(r,\theta,z) = \Phi_0(r,\theta,z) + \Phi_7(r,\theta,z) + \sum_{j=1}^{6} -i\omega\xi_j\Phi_j(r,\theta,z) \quad (2)$$

where $\Phi_0(r,\theta,z)$ represents the velocity potential of the incident wave, $\Phi_7(r,\theta,z)$ represents the diffraction velocity potential, $\Phi_j(r,\theta,z)$ represents the radiation velocity potential of the buoy in the j mode motion, and ξ_j represents the amplitude of the buoy in the j mode motion. $j=3$, in considering only the heave motion of buoy (direction "3"). In the outer watershed around the buoy $E(R \le r \le \infty, -h \le z \le 0)$, its velocity potential is expressed as $\Phi^{\ell,E}(r,\theta,z)$; in the fluid subdomain at the bottom of the buoy $I(0 \le r \le R, -h \le z \le -d)$, its velocity potential is expressed as $\Phi^{\ell,I}(r,\theta,z)$.

Applying the linear plane incident wave with amplitude ξ_0 [30].

$$\begin{aligned} \Phi_0 &= \xi_0 g/i\omega \cdot \sum_{\ell=1}^{\infty} \varphi_0^{\ell}(r,z)\cos\ell\theta \\ \varphi_0^{\ell}(r,z) &= i^{\ell}\varepsilon_{\ell}J_{\ell}(k_0 r)\cosh(k_0(z+h))/\cosh(k_0 h) \quad (\varepsilon_0 = 1, \varepsilon_{\ell} = 2\ (\ell \ge 1)) \end{aligned} \quad (3)$$

Since the diffraction velocity potential is generated by the incident wave acting on a fixed buoy, the space diffraction velocity potential is expressed as follows:

$$\Phi_7(r,\theta,z) = \xi_0 g/i\omega \cdot \sum_{\ell=1}^{\infty} \varphi_7^{\ell}(r,z)\cos\ell\theta \quad (4)$$

On the basis of the Laplace equation, the velocity potential of fluid subdomain E needs to satisfy the free surface condition at the free surface, the bottom boundary condition at the bottom and the radiation condition at infinity.

$$\varphi_7^{\ell,E}(r,z)=\alpha_7^{\ell,E,0}\cosh(k_0(z+h))H_\ell(k_0r)+\sum_{n=1}^{\infty}\alpha_7^{\ell,E,n}\cos(k_n(z+h))K_\ell(k_nr) \tag{5}$$

The velocity potential of fluid subdomain I needs to satisfy the Laplace equation, bottom boundary condition, $\partial_z\varphi_7^{\ell,I}(r,z)=0$ at $z=-d$ and the existence of velocity potential at the centre of a circle. Among them, λ_n denotes the corresponding wavelength of wave number k_n, $\lambda_n=n\pi/h_p$, h_p is the depth between the bottom and the bottom of each surface after discretization, which is shown in Fig.1(c).

$$\varphi_7^{\ell,I}(r,z)=a_7^{\ell,I,0}(r/R)^\ell+\sum_{n=1}^{\infty}a_7^{\ell,I,n}\cos(\lambda_n(z+h))\mathrm{I}_\ell(k_nr) \tag{6}$$

In order to satisfy the continuous condition at the coupling interface($r=R_p,-h\le z\le h_p-h\,(p=1,2...N-1)$, R_p denotes the radius of all surfaces after discretization) and ($r=R,-h\le z\le -t$), which is shown in Fig.1(c). the Galerkin method and the orthogonality of functions are used to obtain the integral equations.

$$\begin{aligned}
\int_{-h}^{h_p-h}\varphi_7^{\ell,I_P}(R_p,z)dz&=\int_{-h}^{h_p-h}\varphi_7^{\ell,I_{P+1}}(R_p,z)dz\\
\int_{-h}^{h_p-h}\varphi_7^{\ell,I_P}(R_p,z)\cos\lambda_n(z+h_p)dz&=\int_{-h}^{h_p-h}\varphi_7^{\ell,I_{P+1}}(R_p,z)\cos\lambda_n(z+h_p)dz\\
\int_{-h}^{h_p-h}\partial_r\varphi_7^{\ell,I_P}(R_p,z)\cosh k_0(z+h)dz&=\int_{-h}^{h_{p+1}-h}\partial_r\varphi_7^{\ell,I_{P+1}}(R_p,z)\cosh k_0(z+h)dz\\
\int_{-h}^{h_p-h}\partial_r\varphi_7^{\ell,I_P}(R_p,z)\cos k_n(z+h)dz&=\int_{-h}^{h_{p+1}-h}\partial_r\varphi_7^{\ell,I_{P+1}}(R_p,z)\cos k_n(z+h)dz\\
\int_{-h}^{-t}\varphi_7^{\ell,I_N}(R,z)dz&=\int_{-h}^{-t}[\varphi_0^{\ell}(R,z)+\varphi_7^{\ell,E}(R,z)]dz\\
\int_{-h}^{-t}\varphi_7^{\ell,I_N}(R,z)\cos\lambda_n(z+h)dz&=\int_{-h}^{-t}[\varphi_0^{\ell}(R,z)+\varphi_7^{\ell,E}(R,z)]\cos\lambda_n(z+h)dz\\
\int_{-h}^{-t}\partial_r\varphi_7^{\ell,I_N}(R,z)\cosh k_0(z+h)dz&=\int_{-h}^{0}\partial_r[\varphi_0^{\ell}(R,z)+\varphi_7^{\ell,E}(R,z)]\cosh k_0(z+h)dz\\
\int_{-h}^{-t}\partial_r\varphi_7^{\ell,I_N}(R,z)\cos k_n(z+h)dz&=\int_{-h}^{0}\partial_r[\varphi_0^{\ell}(R,z)+\varphi_7^{\ell,E}(R,z)]\cos k_n(z+h)dz
\end{aligned} \tag{7}$$

The analytical expression of the diffraction velocity potential of the flow field around a CAB is obtained by solving the integral equations. The vertical dimensionless wave excitation force on a buoy in waves is solved by the Bernoulli equation.

$$\begin{aligned}
F_3=&-i\rho g\xi_0\pi R^2\alpha_7^{0,I_1,0}-\rho g\xi_0\pi R^2\sum_{n=1}^{\infty}\alpha_7^{0,I_1,n}\frac{(-1)^n}{\lambda_nR^2}\frac{\mathrm{I}_0(k_0r)}{\mathrm{I}_0'(k_0R)}\\
&-i2\pi\rho g\xi_0\sum_{p=2}^{N}\left\{\alpha_7^{0,I_p,0}[1-\frac{R_p^2-R_{p-1}^2}{2R_p^2\ln(R_p/R_{p-1})}]\right\}\\
&-i2\pi\rho g\xi_0\sum_{p=2}^{N}\left\{\sum_{n=1}^{\infty}\alpha_7^{0,I_p,n}(-1)^n[\mathrm{K}_I^{n0}\cdot R_p\,\mathrm{I}_1(\lambda_nR_p)/\lambda_n-\mathrm{I}_I^{n0}\cdot R_p\mathrm{K}_1(\lambda_nR_p)/\lambda_n]\right\}\\
&-i2\pi\rho g\xi_0\sum_{p=2}^{N}\left\{\tilde{\alpha}_7^{0,I_p,0}[\frac{R_{p-1}^2}{R_p^2}-\frac{R_p^2-R_{p-1}^2}{2R_p^2\ln(R_p/R_{p-1})}]\right\}\\
&-i2\pi\rho g\xi_0\sum_{p=2}^{N}\left\{\sum_{n=1}^{\infty}\tilde{\alpha}_7^{0,I_p,n}(-1)^n[\mathrm{I}_E^{n0}\cdot R_p\mathrm{K}_1(\lambda_nR_p)/\lambda_n-\mathrm{K}_E^{n0}\cdot R_p\,\mathrm{I}_1(\lambda_nR_p)/\lambda_n]\right\}
\end{aligned} \tag{8}$$

According to the vertical axisymmetric characteristics of the buoy, the radiation velocity potential generated by the heave motion of the buoy is expressed as follows[30]

$$\Phi_3(r,\theta,z)=\varphi_3(r,z) \tag{9}$$

Based on the boundary conditions, the series expressions of heave radiation velocity potential in two kinds of fluid subdomain are obtained by the separation method.

$$\varphi_3^E(r,z)=\alpha_3^{E,0}\cosh(k_0(z+h))H_0(k_0r)+\sum_{n=1}^{\infty}\alpha_3^{E,n}\cos(k_n(z+h))K_0(k_nr) \tag{10}$$

$$\begin{aligned}\varphi_3^{I_p}(r,z)&=\alpha_3^{I_p,0}G_0^{\ell}(r)+\sum_{n=1}^{\infty}\alpha_3^{I_p,n}\left\{\mathrm{K}_I^{n\ell}\cdot\mathrm{I}_{\ell}(\lambda_n r)-\mathrm{I}_I^{n\ell}\cdot\mathrm{K}_{\ell}(\lambda_n r)\right\}\cos\lambda_n(z+h_p)\\&+\tilde{\alpha}_3^{I_p,0}\tilde{G}_0^{\ell}(r)+\sum_{n=1}^{\infty}\tilde{\alpha}_3^{I_p,n}\left\{\mathrm{I}_E^{n\ell}\cdot\mathrm{K}_{\ell}(\lambda_n r)-\mathrm{K}_E^{n\ell}\cdot\mathrm{I}_{\ell}(\lambda_n r)\right\}\cos\lambda_n(z+h_p)+\frac{2(z+h)^2-r^2}{4h_pR}\end{aligned}\tag{11}$$

The integral equations are obtained by coupling the velocity potential at the interface ($r=R_p,-h\le z\le h_p-h\,(p=1,2...N-1)$ and $r=R,-h\le z\le -t$) and the continuous conditions of partial derivatives.

$$\begin{aligned}\int_{-h}^{h_p-h}\varphi_3^{I_p}(R_p,z)dz&=\int_{-h}^{h_p-h}\varphi_3^{I_{p+1}}(R_p,z)dz\\\int_{-h}^{h_p-h}\varphi_3^{I_p}(R_p,z)\cos\lambda_n(z+h)dz&=\int_{-h}^{h_p-h}\varphi_3^{I_{p+1}}(R_p,z)\cos\lambda_n(z+h)dz\\\int_{-h}^{h_p-h}\partial_r\varphi_3^{I_p}(R_p,z)\cosh k_0(z+h)dz&=\int_{-h}^{h_{p+1}-h}\partial_r\varphi_3^{I_{p+1}}(R_p,z)\cosh k_0(z+h)dz\\\int_{-h}^{h_p-h}\partial_r\varphi_3^{I_p}(R_p,z)\cos k_n(z+h)dz&=\int_{-h}^{h_{p+1}-h}\partial_r\varphi_3^{I_{p+1}}(R_p,z)\cos k_n(z+h)dz\\\int_{-h}^{-t}\varphi_3^{I_p}(R,z)dz&=\int_{-h}^{-t}\varphi_3^{E}(R,z)dz\\\int_{-h}^{-t}\varphi_3^{I_p}(R,z)\cos\lambda_n(z+h)dz&=\int_{-h}^{-t}\varphi_3^{E}(R,z)\cos\lambda_n(z+h)dz\\\int_{-h}^{-t}\partial_r\varphi_3^{I_p}(R,z)\cosh k_0(z+h)dz&=\int_{-h}^{0}\partial_r\varphi_3^{E}(R,z)\cosh k_0(z+h)dz\\\int_{-h}^{-t}\partial_r\varphi_3^{I_p}(R,z)\cos k_n(z+h)dz&=\int_{-h}^{0}\partial_r\varphi_3^{E}(R,z)\cos k_n(z+h)dz\end{aligned}\tag{12}$$

By solving the integral equations, the analytical expression of the radiation velocity potential around the buoy due to the slight heave motion of the buoy is obtained. The vertical radiation force acting on the buoy is solved by the Bernoulli equation.

$$F_{33}=-i2\rho\pi d\sum_{p=1}^{N}\int_{R_{p-1}}^{R_p}\varphi_3^{I_p}(r,h_p-h)rdr\tag{13}$$

The radiation forces, coming from the buoy's motion, are decomposed into velocity and acceleration components. The dimensionless adds mass and radiation damping coefficients in the vertical axis are:

$$\begin{aligned}\mu_{33}+i\lambda_{33}/\omega=&-i\rho\pi R^2 d\alpha_3^{I_1,0}-\rho\pi R^2 d\sum_{n=1}^{\infty}\alpha_3^{I_1,n}\frac{(-1)^n}{\lambda_n R_1^2}\frac{\mathrm{I}_0(k_0r)}{\mathrm{I}_0^{'}(k_0R)}\\&-i2\rho\pi d\sum_{p=2}^{N}\left\{\alpha_3^{I_p,0}[1-\frac{R_p^2-R_{p-1}^2}{2R_p^2\ln(R_p/R_{p-1})}]\right\}\\&-i2\rho\pi d\sum_{p=2}^{N}\left\{\sum_{n=1}^{\infty}\alpha_3^{I_p,n}(-1)^n[\mathrm{K}_I^{n0}\cdot R_p\,\mathrm{I}_1(\lambda_n R_p)/\lambda_n-\mathrm{I}_I^{n0}\cdot R_p\mathrm{K}_1(\lambda_n R_p)/\lambda_n]\right\}\\&-i2\rho\pi d\sum_{p=2}^{N}\left\{\tilde{\alpha}_3^{I_p,0}[\frac{R_{p-1}^2}{R_p^2}-\frac{R_p^2-R_{p-1}^2}{2R_p^2\ln(R_p/R_{p-1})}]\right\}\\&-i2\rho\pi d\sum_{p=2}^{N}\left\{\sum_{n=1}^{\infty}\tilde{\alpha}_3^{I_p,n}(-1)^n[\mathrm{I}_E^{n0}\cdot R_p\mathrm{K}_1(\lambda_n R_p)/\lambda_n-\mathrm{K}_E^{n0}\cdot R_p\,\mathrm{I}_1(\lambda_n R_p)/\lambda_n]\right\}\end{aligned}\tag{14}$$

2.2 Dynamic characteristics of the CAB-WEC in the frequency domain

A PAWEC generally includes an energy-absorbing buoy, PTO system and carrier. It utilizes the reciprocating relative motion of buoy and carrier to output energy by driving the PTO. Fig. 2(a) shows the energy absorption principle of the PAWEC. PTO devices are divided into hydraulic, pneumatic, mechanical and direct drive. Hydraulic transmission in hydraulic PTO has the advantages of small inertia, stable output and high conversion efficiency. For the damping characteristics of the hydraulic PTO system of the PAWEC, a linear damping system is often applied, ignoring the non-linear effect. Meanwhile, the damping of the hydraulic cylinder is limited to a time-invariant coefficient. Since there is no stiffness coefficient of the hydraulic cylinder and the recovery spring is corroded when exposed to Seawater, considering that the main function of the recovery spring is to prevent the buoy from colliding or detaching from the base, the hydraulic cylinder can achieve the function, and generally a recovery spring is not installed. Therefore, without considering the optimization of buoy size, the damping

coefficient of the hydraulic cylinder is the only control variable in the first stage energy absorption process of the device. In order to eliminate the mechanical friction caused by the fixing buoy, mooring weight is used to restrict the motion of surge and pitch degrees of freedom. Fig. 2(b) shows the schematic diagram of the experimental method. The PTO device in Fig. 2 restricts the motion of the buoy only in the direction "3" (heave). Therefore, only the motion of the float in this direction is considered in the calculation.

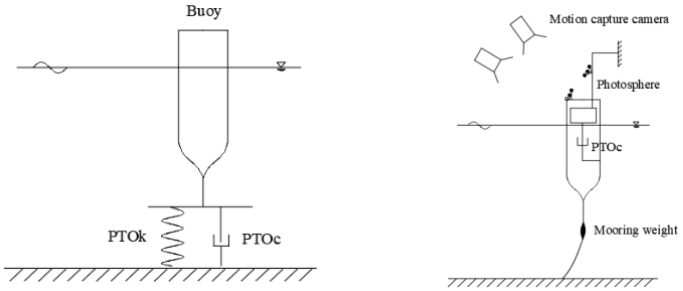

(a) Device schematic diagram (b) Experimental schematic diagram

Fig. 2. Device and experimental schematic diagram

The equation of the motion of a buoy with a PTO system in the frequency domain is expressed as follows[31]: .

$$m\ddot{X} = F_{\mathrm{D}} + F_{\mathrm{R}} + F_{\mathrm{C}} + F_{M} \tag{15}$$

Hydrostatic resilience is expressed as follows:

$$F_{\mathrm{C}} = -\rho g s X \tag{16}$$

Radiation force is decomposed into two parts related to acceleration and velocity.

$$F_{R} = F_{R}^{\ a} + F_{R}^{\ d} = -\ddot{X}\mu - \dot{X}\lambda \tag{17}$$

Under the condition of linear damping(α=0), the action of the PTO on appendages is expressed as follows: c denotes the PTO damping coefficient.

$$F_{M} = -c\dot{X} \tag{18}$$

By substituting F_{C}, F_{R} and F_{M} into the equation of motion of a buoy, the equation of motion in the frequency domain introduced into the linear PTO system is obtained.

$$(m+\mu)\ddot{X} + (\lambda + \mathrm{c})\dot{X} + \rho g s X = F_{\mathrm{D}} \tag{19}$$

In the frequency domain analysis, it is considered that the buoy and the incident wave move periodically at the same frequency, and the time variables of the velocity potential and its related physical quantities are separated.

$$[\Psi, F, X, P](x, y, z, t) = \mathrm{Re}\left\{[\Phi, f, \chi, p](x, y, z)e^{-i\omega t}\right\} \tag{20}$$

The time variables of the amplitude of the pendulum motion of the linear PTO system can be separated by the above formula.

$$\chi = f_{D}/\{-\omega^{2}(m+\mu) - i\omega(\lambda + c) + \rho g s\} \tag{21}$$

In frequency domain analysis, the average value of the external force power of the PTO damper system in a period is expressed as follows[31]: .

$$\bar{P} = \frac{1}{T}\int_{0}^{T} F\dot{X}dt \tag{22}$$

where F represents the force acting on the PTO device. In this paper, F equals to F_{M} .

Average output power of WEC with PTO is obtained by separating the time term.

$$\bar{P}_{c} = \frac{1}{2}c\omega^{2}\chi\chi^{*} \tag{23}$$

Add the amplitude of the buoy pendulum motion to the average output power.

$$\bar{P}_{c} = \frac{1}{2}\omega^{2} f_{D} f_{D}^{\ *} \frac{c}{[-\omega^{2}(m+\mu) + \rho g s]^{2} + [\omega(\lambda + c)]^{2}} \tag{24}$$

The capture width ratio represents the ratio of the average output power of the buoy to the regular incident wave power in the width of the buoy.

$$\eta_{\mathrm{p}} = P_{c}(\omega_{j})/P_{0}(\omega_{j}) \tag{25}$$

$P_{0}(\omega_{j})$ is the regular incident wave power in unit period of the frequency as ω_{j} and buoy width of CAB. According to the Bernoulli equation, the regular incident wave velocity potential is integrated, and the dispersion relation $gk_{j}\tanh k_{j}h = \omega_{j}^{2}$ is introduced. The input energy of incident wave in unit period and float width is obtained as follows:

$$P_0(\omega_j) = \rho g^2 RA(\omega_j)^2 / (2\omega_j) \cdot (2k_j h + \sinh 2k_j h) / (1 + \cosh 2k_j h) \quad (26)$$

Among them, $A(\omega_j)$ is expressed as wave amplitude and k_j is indicated as wave number.

2.3 PTO optimization of CAB-WEC in the frequency domain

In the previous section, the expression of the capture width ratio on the CAB is given. The expression shows that when the buoy and frequency are constant, the hydrodynamic coefficient of the buoy and the incident wave power in the width of the buoy are fixed values. The PTO damping coefficient is the only variable of the capture width ratio. That means the optimization of PTO is equivalent to the analysis of the relationship between the PTO damping coefficient and capture width ratio.

Since the incident wave power in the width of the buoy is independent of the PTO damping coefficient, the optimal capture width ratio is to find the maximum of the average output power of the WEC with respect to the PTO damping coefficient, so the partial derivative of c in $\bar{P}_c$ is obtained.

$$\partial_c \bar{P}_c = 0 \quad (27)$$

The optimal PTO damping coefficient and frequency relation for linear PTO system are obtained by calculation.

$$c_{optimal} = \sqrt{\left[-\omega^2(m+\mu) + \rho g s\right]^2 \Big/ \omega^2 + \lambda^2} \quad (28)$$

The optimal PTO damping coefficient obtained is the maximum point of the curve of the capture width ratio varying with the PTO damping coefficient at a certain frequency. The expression of the optimal damping coefficient shows that it is related to the frequency and the hydrodynamic coefficient of the buoy. When the size of the buoy is fixed, each frequency corresponds to the certain optimal PTO damping coefficient.

The optimal damping coefficient is introduced into the expression of capture width ratio. The maximum of the capture width ratio of the WEC of the PTO system is expressed as follows:

$$\eta_{\mathrm{p}}^{\max} = \bar{P}_c^{\max} / P_0 = \omega f_D f_D^* \Big/ \{4P_0(\sqrt{[-\omega^2(m+\mu) + \rho g s]^2 + \omega^2\lambda^2} + \omega\lambda)\} \quad (29)$$

The maximum capture width ratio obtained is the maximum of the curve of the capture width ratio varying with PTO damping coefficient at a certain frequency.

2.4 Numerical solution of dynamic characteristics of the CAB-WEC in the time domain under irregular waves by IRF method

Based on the frequency domain potential flow theory, IRF method is used to transform the frequency domain results into time domain results. The International Ship Structure Congress (ISSC) wave spectrum is selected and the wave force and hydrodynamic coefficients obtained by frequency domain analysis are used to establish the time domain motion control equation to solve the time domain motion characteristics of the wave energy float and the potential current time domain solution of energy conversion under irregular waves.

The equation of motion of a buoy with a PTO system in the time domain is expressed as follows[31]:

$$M\ddot{X}(t) = F_{\mathrm{D}}(t) + F_{\mathrm{R}}(t) + F_{\mathrm{C}}(t) + F_{\mathrm{M}}(t) \quad (30)$$

Hydrostatic resilience is expressed as follows:

$$F_C = -\rho g s X(t) \quad (31)$$

The radiation force is expressed by impulse response function, where m and $\mathrm{K}(\cdot)$ are additional mass in time domain and delay functions, respectively. When $\omega \to +\infty$, $m = \mu(+\infty)$, $K(\tau) = \frac{2}{\pi}\int_0^{+\infty} G(\omega,\tau)\mathrm{d}\omega$, where $G(\omega,\tau) = \lambda_{33}(\omega)\cos(\omega\tau)$, $\lambda_{33}(\omega)$ represents the radiation damping of the "3" direction of the CAB at different wave frequencies, which can be calculated by Eq.(14).

$$F_{\mathrm{R}}(t) = -m \cdot \ddot{X}(t) - \int_0^t \dot{X}(\tau)\mathrm{K}(t-\tau)\mathrm{d}\tau \quad (32)$$

Under the condition of linear damping, the action of PTO on appendages is expressed as follows:

$$F_M = -c\dot{X}(t) \quad (33)$$

By substituting $F_{\mathrm{C}}(t)$, $F_{\mathrm{R}}(t)$ and F_M into the equation of motion of a buoy, the equation of motion in the time domain introduced into the linear PTO system is obtained.

$$(M+m)\ddot{X}(t) + \int_0^t K(t-\tau)\dot{X}(\tau)d\tau + \rho g s X(t) = F_{\mathrm{D}}(t) - c\dot{X}(t) \quad (34)$$

The wave spectrum of irregular waves is introduced into the equation of motion of a buoy in the time domain

by wave loads[32]. $\Delta\omega$ denotes the frequency step and δ_j denotes the random phase.

$$\mathrm{F}_D(t)=\sum_{i=1}^{\infty}\left|F_d(\omega_i)A(\omega_i)\sin(\omega_i t+\delta_i)\right| \tag{35}$$

$$\mathrm{A}(\omega_i)=\sqrt{2S(\omega_i)\Delta\omega} \tag{36}$$

ISSC wave spectrum is used, in which H_s denotes the significant wave height and T_p denotes the peak period.

$$\mathrm{S}(\omega,H_s,T_p)=H_s^2\cdot(0.7713T_p)\frac{0.11}{2\pi}\left(\frac{\omega\cdot(0.7713T_p)}{2\pi}\right)^{-5}exp\left[-0.44\left(\frac{\omega\cdot(0.7713T_p)}{2\pi}\right)^{-4}\right] \tag{37}$$

The power expression of the external force of the instantaneous linear PTO damper system is expressed as follows:

$$P(t)=c\dot{X}^2(t) \tag{38}$$

In irregular waves, when the structure of WEC device is determined, the capture width ratio of the WEC is regarded as a function of the significant wave height and spectral peak period. Referring to the capture width ratio under regular waves, $P(H_s,T_p)$ is the capture energy $P(t)$ of the device under irregular waves with significant wave height H_s and peak period T_p.

$$\eta=\frac{\int_0^T P(H_s,T_p,t)dt}{P_0(H_s,T_p)T}=\frac{\int_0^T\frac{P(H_s,T_p,t)}{P_0(H_s,T_p)}dt}{T}=\frac{\int_0^T\eta_p(H_s,T_p,t)dt}{T} \tag{39}$$

$$P_0(H_s,T_p)=\sum_{j=1}^{N}\rho g^2R\omega_jA_j^2(H_s,T_p)/(2\omega_j)\cdot(2k_jh+\sinh 2k_jh)/(1+\cosh 2k_jh) \tag{40}$$

In order to calculate the equation of motion in the time domain, let $y_1(t)=X(t);\ y_2(t)=\dot{X}(t)$. $X(t)$ represents the instantaneous surge motion response of the CAB; $y_1(t)$ represents the instantaneous surge motion velocity of the CAB; $y_2(t)$ represents the instantaneous surge motion acceleration of the CAB. A first-order differential equation system is obtained by introducing the motion equation in the time domain.

$$\begin{cases}\dot{y}_1=y_2 & y_1(0)=0\\ \dot{y}_2=\dfrac{F_{\mathrm{E}}(t)-ky_1-\int_0^t K(t-\tau)y_2(\tau)d\tau}{M+m} & y_2(0)=0\end{cases} \tag{41}$$

The above first-order differential equation system can be solved by fourth-order Runge-Kutta iteration.

2.5 PTO control of CAB-WEC in the time domain under irregular waves

The optimization of the PTO damping coefficient under irregular waves in the time domain is to increase the capture width ratio of the device by changing the PTO damping coefficient. However, the capture width ratio varies with time in the time domain analysis. In other words, the capture ratio in the time domain is a non-constant value. The ratio of capture width under regular waves has a stable extremum, i.e., the ratio of capture width in frequency domain, while the ratio of capture width under irregular waves does not follow the same phenomenon as regular wave conditions. In order to measure the performance of the wave energy capture device in the time domain, the concept of an average capture width ratio is introduced, in which T_{MAX} denotes the sufficiently long period of time. The average capture width ratio in this period is close to the value in infinite time. The key to this measurement standard is the determination of T_{MAX}. According to Eq.(40), the irregular wave can be regarded as the superposition of numerous regular waves. $P_0(H_s,T_p)$ are independent of the time term. That means $P_0(H_s,T_p)$ is not a function of time. Therefore, $\int_0^{T_{MAX}}P_0(H_s,T_p)dt=P_0(H_s,T_p)T_{MAX}$.

$$\overline{\eta_p}(T_{MAX})=\frac{\int_0^{T_{MAX}}P(t)dt}{\int_0^{T_{MAX}}P_0(H_s,T_p)dt}=\frac{\int_0^{T_{MAX}}P(t)dt}{P_0(H_s,T_p)T_{MAX}}=\frac{\int_0^{T_{MAX}}\frac{P(t)}{P_0(H_s,T_p)}dt}{T_{MAX}}=\frac{\int_0^{T_{MAX}}\eta_p(t)dt}{T_{MAX}} \tag{42}$$

On the basis of the ISSC wave spectrum, the instantaneous capture width ratio of the PTO system under different PTO damping coefficients is calculated under different wave conditions in the time domain, and the

average capture width ratio of the PTO system in the time domain is thus obtained.

The numerical optimization of the PTO damping coefficient under irregular waves in the time domain is to fit the relationship curve between the average capture width ratio and the PTO damping coefficient in T_{MAX} by calculating the average capture width ratio under multiple groups of PTO damping coefficients. Based on the analysis of the curve, the maximum value of the curve is obtained by dichotomy, i.e., the optimal PTO damping coefficient under this kind of wave condition. In time domain analysis, the significant wave height does not affect the capture width ratio in the same spectral peak period. Therefore, the wave condition can be changed merely by the numerical value of the spectral peak period.

3. Numerical Results and Discussion

3.1 Verification of hydrodynamic coefficients

In order to verify the analytical solutions, HydroSTAR hydrodynamic calculation software is adopted for comparison calculation. The parameters are the same as the above-mentioned CAB, The bottom shape of the CAB is divided into two parts: the upper half of the buoy is a cylinder with radius $r = 1m$, and the lower half shape is based on the BW (Berkeley Wedge) curve. The total draft of CAB is selected as $d = 5m$, and the total length of the CAB is selected as $L = 6m$. The seabed is horizontal, water depth $h = 50m$, sea density $\rho = 1025kg/m^3$, gravity acceleration $g = 9.81m/s^2$ are selected. Table 1 shows the comparison of wave forces and droop hydrodynamic coefficients calculated by the present method and HydroSTAR. The numerical results show that the existing analytical solutions are in good agreement with the HydroSTAR calculation. Relative error is kept within 1%. The methodology here proposed can be considered verified.

Table 1 Verification of the solution method

$\omega(rad/s)$	0.5			1			1.5		
	Present	HydroSTAR	E_r	Present	HydroSTAR	E_r	Present	HydroSTAR	E_r
Wave force f_D (KN)	27.92	28.17	0.9 %	19.17	19.36	1.0 %	10.25	10.32	0.7 %
Added mass μ (kg)	1743.5	1754.0	0.6 %	1623.9	1630.4	0.4 %	1503.8	1511.3	0.5 %
Damping λ $(KN/(m/s))$	48.62	48.96	0.7 %	193.65	195.39	0.9 %	186.96	188.64	0.9 %

3.2 Dynamic characteristics of the CAB-WEC in the frequency domain

According to the expression of motion response and capture width ratio in the frequency domain, the semi-analytical solution of wave force, additional mass and radiation damping coefficient with the CAB are used to calculate the motion response and capture width ratio of the CAB under a linear PTO damping system in the frequency domain, and the influence of different damping coefficients on the motion characteristics and capture width ratio of wave energy devices are studied. The incident wave amplitude $A = 1m$ and the circular frequency $\omega = 0.5,1.0,1.5,2.0,2.5(\text{rad/s})$ are selected.

Fig. 3(a) shows the variation curves of CAB motion response under different damping coefficients. Under a given frequency, when the damping coefficient is small, the corresponding motion response of the buoy decreases rapidly. With the increase of the damping coefficient, the reduction rate of the motion response decreases gradually until it approaches zero. When the damping coefficient falls in the range of $c = 20 \sim 50kN/(m/s)$, the corresponding motion response decreases more rapidly with the increase of the damping coefficient. When the damping coefficient is $c = 20 \sim 250kN/(m/s)$, the corresponding motion response decreases with the increase of incident wave frequency. Fig. 3(b) shows the curves of the CAB capture width ratio under different damping coefficients. The average output power increases from zero, then decreases to zero after reaching the peak value. Comparing the five curves in the figure, the capture width ratio peaks at different frequencies are ranked as $\omega = 1.5,2.0,1.0,2.5,0.5(\text{rad/s})$ from small to large. The damping coefficients corresponding to the capture width ratio peak at different frequencies are ranked as $\omega = 2.5,2.0,0.5,1.0,1.5(\text{rad/s})$ from small to large.

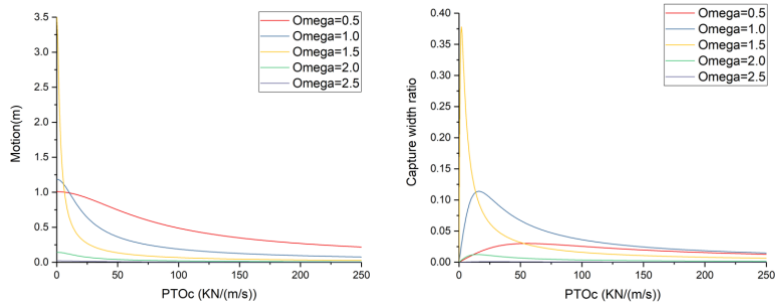

(a) Motion (b) Capture width ratio

Fig. 3. Curve of dynamic characteristics versus PTO damping coefficient

3.3 PTO optimization of the CAB-WEC in the frequency domain

In order to verify the correctness of the optimal PTO damping coefficient under the linear PTO system, the curves of the capture width ratio varying with the PTO damping coefficient at different frequencies are calculated with the same buoy in terms of hydrodynamic coefficients. Fig. 4 shows the curve of the optimal PTO damping coefficient under different circular frequencies (ω=1.1,1.2,1.3,1.4,1.5rad/s). Each curve has a maximum value, and the maximum point is the optimal PTO damping coefficient. The maximum points are calculated by dichotomy, which are $11.78KN/(m/s)$,$7.88KN/(m/s)$,$4.35KN/(m/s)$,$1.12KN/(m/s)$,$1.92KN/(m/s)$. Fig. 5 shows the optimal PTO damping coefficient of the float varying with frequency. The maximum point of Fig. 4 in each frequency coincides with the curve of Fig. 5, which proves that the optimal PTO damping coefficient maximizes the capture width ratio.

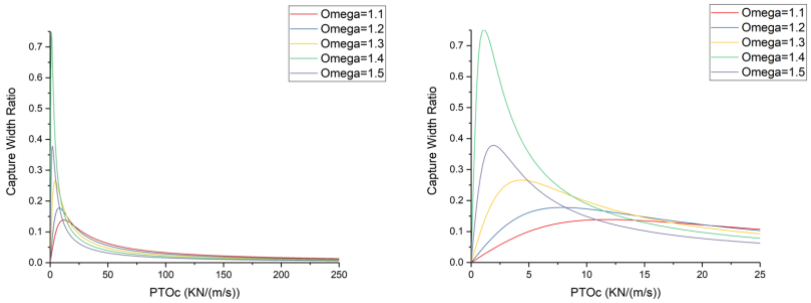

(a)0~250KN/(m/s) (b) 0~25KN/(m/s)

Fig. 4. Curve of capture width ratio versus PTO damping coefficient

Fig. 5 shows that there is a minimum point in the optimal PTO damping coefficient curve. When ω=0~0.1rad/s , the optimal PTO damping coefficient changes dramatically. On both sides of the extreme point, the absolute value of the curve slope decreases gradually. This means that with the decrease of frequency, the change of the optimal PTO damping coefficient becomes more intense at the left side of the extremum, and more gentle at the right side of the extremum.

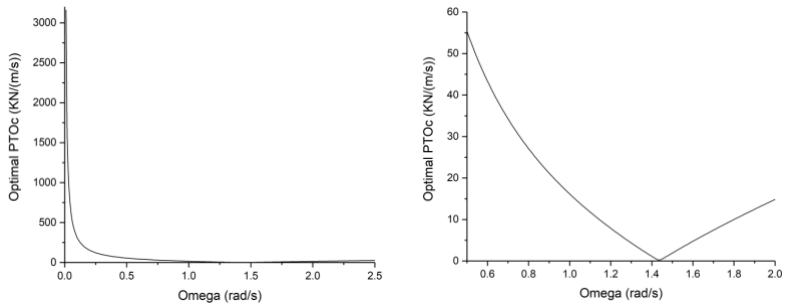

(a)0~2.5rad/s (b) 0.5~1.5rad/s

Fig. 5. Curve of optimal PTO damping coefficient versus frequency

3.4 Dynamic characteristics of the CAB-WEC in the time domain in irregular waves

The impulse response function method is adopted to calculate the hydrodynamic coefficients obtained by frequency domain analysis, and the time domain motion response and capture width ratio under irregular waves are calculated. The calculated parameters are the same as those in the frequency domain, and the PTO damping coefficient is $10KN/(m/s)$.

Fig. 6 shows the curves of motion response with time under different wave conditions. Comparing Fig. 6 (a) with (b), the variations in the motion response images with different significant wave heights are identical in the same spectral peak periods, but the corresponding regulations are discrepant. Comparing Fig. 6 (b) with (c), the variations in the motion response images with different spectral peak periods are discrepant to the same significance. In order to ensure the reasonableness of the conclusion, multiple groups of the motion for different spectral peak periods and significant wave heights are also calculated. All of them reach the same conclusion as above. To sum up, for the motion response, the significant wave height determines the size of the numerical value, and the spectral peak period determines the variation of the image.

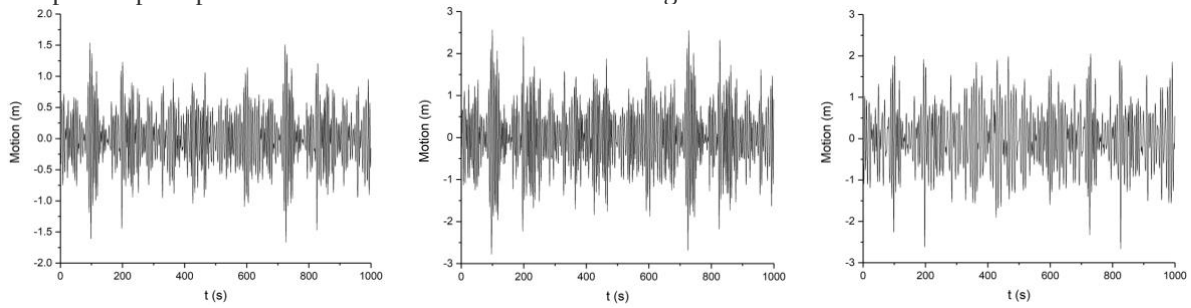

(a) $H_s = 2m, T_p = 6s$ (b) $H_s = 3m, T_p = 6s$ （c） $H_s = 3m, T_p = 8s$

Fig. 6. Time-history curve of motion under different wave conditions

Fig. 7 shows the curves of capture width ratio with time under different wave conditions. Comparing Fig. 7(a) with (b), the images of capture width ratio with different significant wave heights are identical in the same spectral peak periods. Comparing Fig. 7(b) with (c), the variations in the capture width ratio images with different spectral peak periods are discrepant to the same significance. In order to ensure the reasonableness of the conclusion, multiple groups of the capture width ratio in different spectral peak periods and significant wave heights are also calculated. All of them reach the same conclusion as above. To sum up, for the capture width ratio, the significant wave height has no effect, and the spectral peak period determines the variation of the image.

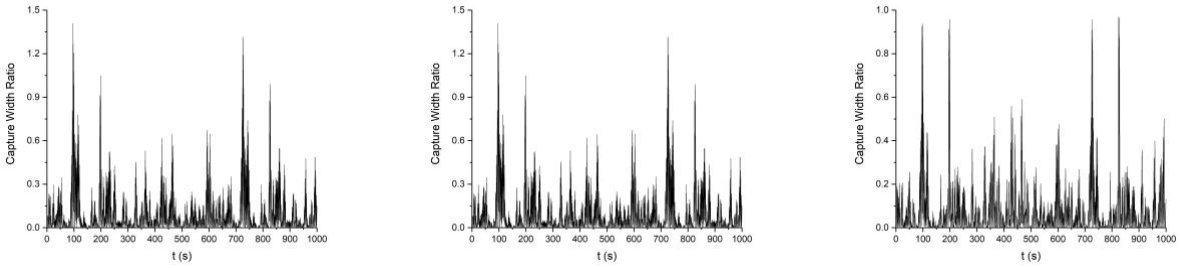

(a) $H_s = 2m, T_p = 6s$ (b) $H_s = 3m, T_p = 6s$ （c） $H_s = 3m, T_p = 8s$

Fig. 7. Time-history curve of capture width ratio under different wave conditions

3.5 PTO control of the CAB-WEC in the time domain under irregular waves

Fig. 8(a) and (b) shows the variation curve of the average capture width ratio with the PTO damping coefficient at different T_{MAX} when the spectral peak period is $6s$. When the T_{MAX} adopts $1000s$ or $2000s$, the calculated average capture width ratios have the same values and the same extremum intervals, and the average errors are within 10^{-2}. Therefore, the choice of T_{MAX} =$1000s$ is reasonable.

Fig. 8 shows the curves of the average capture width ratio with PTO damping coefficient under different wave conditions. Comparing Fig. 8(a), (b) and (c), they indicate that the trend of the curve increases first and then decreases when T_p =$6s$、$8s$、$10s$, thus judging the existence of a maximum value of the curve. Moreover, the average capture width ratio near the maximum point changes gently, and the gentle region widens with the increase of the

maximum point. When T_p=6s, the extremum exists between $5KN/(m/s)$ and $10KN/(m/s)$. In this interval, the optimal PTO damping coefficient is $6.5KN/(m/s)$ by dichotomy. The average capture width ratio is 0.1008, and the accuracy reaches four significant digits. Similarly, when T_p=8s, the optimal PTO damping coefficient is $18.8KN/(m/s)$, the average capture width ratio is 0.8489, and the accuracy reaches three significant digits. When T_p=10s, the optimal PTO damping coefficient is $28KN/(m/s)$, the average capture width ratio is 0.7407, and the accuracy reaches three significant digits.

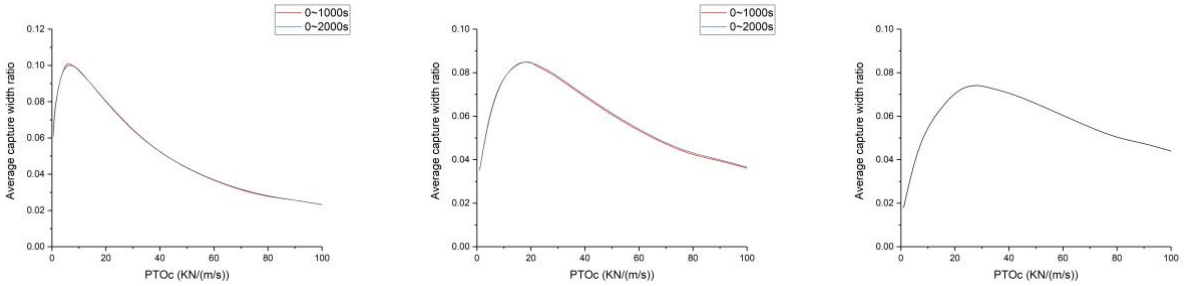

(a) $T_p = 6s$ (b) $T_p = 8s$ （c） $T_p = 10s$

Fig. 8. Curves of the average capture width ratio versus PTO damping coefficient in different wave conditions

The optimal damping coefficients and corresponding average capture width ratios are calculated by the time domain optimization method under multi-group wave conditions with spectral peak periods ranging from 4s to 12s. Fig. 9 shows the time domain optimization characteristics of the CAB under different wave conditions. When $T_p = 4s \sim 12s$ ($\omega_p = 0.52rad/s \sim 1.57rad/s$), with the increase of spectral peak period, the optimal PTO damping coefficient increases gradually, and its variation trend is similar to that of the optimal PTO damping coefficient curve in the frequency domain. The optimal average capture width ratio has a maximum value near 0.11, with the extreme point near 5.5s .Therefore, when selecting the sea area for deploying this kind of CAB, the average spectral peak period should between 5s and 6s.

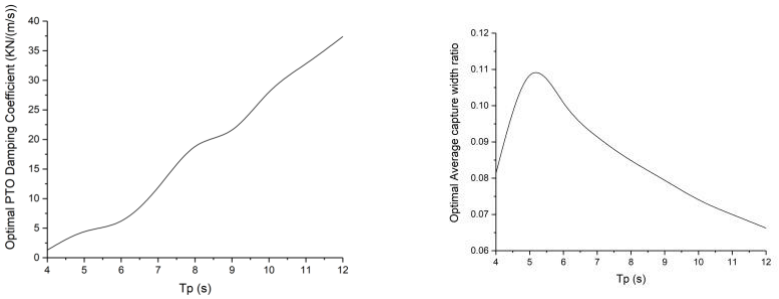

(a) Optimal PTO Damping Coefficient (b) Optimal Average capture width ratio

Fig. 9. Curve of time domain optimization characteristics under different wave conditions

3.6 Comparison of PTO control in the time domain and PTO optimization in the frequency domain

In engineering, the linear control method is usually adopted to optimize the constant PTO damping coefficient. It is considered that the spectral peak frequency of the specified sea area is a long-term statistical value, and the damping coefficient is adjusted to keep the optimal value at the current spectral peak frequency of the wave spectrum. The damping coefficient is a function of the spectral peak frequency, which can be calculated by the spectral peak period. The optimum value of the PTO damping coefficient at a spectral peak frequency of the wave spectrum is obtained by the frequency domain analysis. The optimal PTO damping coefficients at different frequencies are calculated by an analytical method. The PTO is optimized by the optimal damping coefficient curve and spectral peak frequency of the wave spectrum. This method can be regarded as a frequency domain optimization method.

The optimal PTO damping coefficient can be obtained by interpolating the relationship curve between the frequency and the optimal damping coefficient in the frequency domain. The average capture width ratio under the

optimal PTO damping coefficient is calculated and compared with the optimal solution in the time domain. Table 2 shows the optimal PTO damping coefficients in the frequency domain and time domain under different wave conditions. In Table 2. PTOc represents PTO damping coefficient. Compared with the linear control method, the average capture width obtained by the time domain optimization method is better, but the extremum is close to that of the linear control method. The optimum PTO damping coefficients differ greatly, and the difference between the two optimum PTO damping coefficients augments with the increase in the spectral peak period.

The average capture width ratio obtained by using the optimal damping coefficient in the frequency domain is similar to that obtained in the time domain, and it is difficult to solve the functional relationship of the optimal PTO damping coefficient in the time domain analysis Therefore, in practical engineering applications, it is reasonable to obtain the PTO damping coefficient of the device by referring to the optimal damping coefficient curve in frequency domain with the measured spectral peak period.

Table 2 Optimal PTO damping coefficient in frequency and time domain

$T_p(s)$	6			8			10		
	Optimal PTOc $(KN/(m/s))$	$\overline{\eta}_p$	E_r	*Optimal PTOc* $(KN/(m/s))$	$\overline{\eta}_p$	E_r	*Optimal PTOc* $(KN/(m/s))$	$\overline{\eta}_p$	E_r
Frequency Domain	14.02	0.0908	11%	28.04	0.0798	6.2%	40.51	0.0707	4.8%
Time Domain	6.2	0.10080		18.8	0.0848		28	0.0741	

3.7 Comparison of numerical results and experimental dates

In order to verify the time domain optimization method and the time domain optimization curve variation discussed in section 3.5 under different wave conditions, a pool model test was adopted. Firstly, the average capture width ratio of the system under different PTO damping coefficients is measured when $T_p = 6s$; secondly, the average capture width ratio of the system is measured under different wave conditions($T_p = 6s、7s、8s、9s、10s$) when the PTO damping coefficient equals the theoretical optimal value. The characteristic length scale ratio of the experiment is λ=4:1; γ=1025 is the ratio of seawater to freshwater density. The diameter of the float model is $0.5m$, and the total draft of the CAB-WEC is $1.25m$. In the experiment, the CAB-WEC includes CAB, internal PTO system and mooring weight block. The internal PTO system mainly consists of electromagnetic damper, reducer, pulley and mass block. The PTO damping coefficient can be changed by adjusting the electromagnetic damper. The buoy connects the mooring weight block by a wire rope tied to the tip to restrict the motion of surge and pitch degrees of freedom. The mooring weight block is designed in a vertical, streamlined shape to reduce the viscous energy dissipation in the heave direction. The internal mass block is fixed on the trailer and connected to the buoy through the PTO system. Fig. 10 shows the equipment and experiment photographs of the pool model test. The mooring system keeps the CAB-WEC in the designated position, and adopts the wave maker to generate the motion of the buoy. Through the non-contact optical motion measurement system QUALISYS, the external buoy motion and the relative motion of the internal mass block are measured. Finally, the average capture width ratio under different conditions is calculated by adopting the formulas of the motion curve with the time recorded by the data acquisition system.

(a) Towing tank and trailer (b) Wave maker (c) Experiment photograph

Fig. 10. Equipment and experiment photographs of the wave model test

Fig. 11 shows the ratio of the average capture width to the optimal average capture width ratio converted by the similarity criterion. When $T_p = 6s$, the variation trend of the average capture width ratio under different PTO damping coefficients is similar to the theoretical analysis by changing the parameters of the PTO system, which

verifies the correctness of the time domain damping coefficient optimization method. By changing the different wave conditions produced by the wave maker, the optimal average capture width ratio under the optimal PTO damping coefficient is measured to be in good agreement with the theoretical results, which verifies the correctness of the variation in the optimal average capture width ratio.

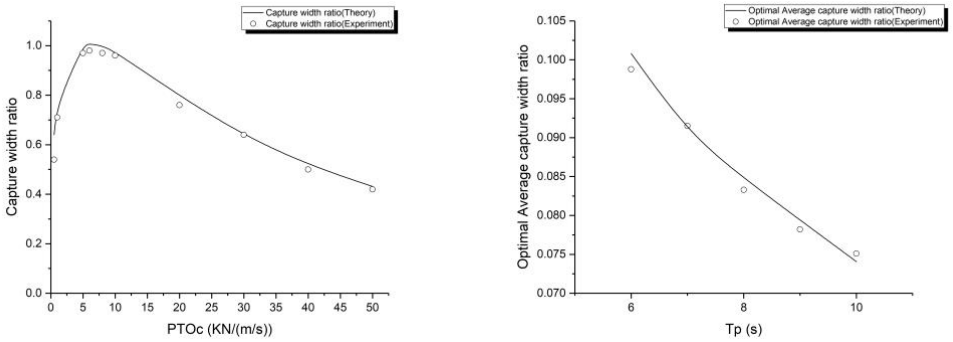

(a) Average capture width ratio($T_p = 6s$) (b) Optimal Average capture width ratio

Fig. 11. Comparison of experimental and theoretical results

4. Conclusions

In this paper, the optimization of a PTO system in the frequency and time domains for a CAB-WEC is investigated. A time domain numerical optimization method is proposed under irregular wave conditions. The relationship between the average capture width ratio and the PTO damping coefficient under different irregular waves is obtained by establishing the criterion of the capture width ratio. To achieve the maximum average capture width ratio, the optimal PTO damping coefficient under different wave conditions is solved. The expression of the optimal PTO damping coefficient in the frequency domain is given. By comparing the linear control method with the time domain optimization method, the relationship between time domain optimization and frequency domain optimization is analysed. Finally, the experimental results verify the correctness of the time domain optimization method and the variation in optimal average capture width ratio.

The results indicate:

[1] There is an optimal PTO damping coefficient for the average capture width ratio under each spectral peak period in the time domain. The change in average capture width ratio near the optimal PTO damping coefficient is gentle, and the gentle region widens with the increase of the optimal PTO damping coefficient.

[2] The optimization results of the average capture width ratio under irregular waves in the time domain are greater than those of the linear control method, but the differences between both are about 10%. Therefore, in engineering, it is reasonable to obtain the PTO damping coefficient of the device by referring to the optimal damping coefficient curve in the frequency domain with the measured spectral peak period.

[3] When $T_p = 4s \sim 12s$, with the increase of spectral peak period, the optimal PTO damping coefficient increases gradually, and its variation trend is similar to that of the optimal PTO damping coefficient curve in the frequency domain. The optimal average capture width ratio has a maximum value near 0.11, with the extreme point near $5.5s$ .Therefore, when selecting the sea area for deploying this kind of CAB, the average spectral peak period should between $5s$ and $6s$.

Acknowledgements

This paper is financially supported by the National Natural Science Foundation (Grant No. 51509048 and No.5197090345), Heilongjiang provincial fund (Grant No.E2017016), State Key Laboratory of Ocean Engineering (Shanghai Jiao Tong University) (Grant No.1703), Harbin Engineering University of basic university basic scientific research business special funds: (HEUCFP 201733), Marine Equipment and Technology Institute, Jiangsu University of Science and Technology (Grant No. HZ20180009) and the Fundamental Research Funds for the Central Universities (Grant No. HEUCFG201828 and No. HEUCFG201808).

References

[1] Miles J W, Gilbert F. Scattering of gravity waves by a circular dock[J]. Journal of Fluid Mechanics, 2006,34(4):

783-793
[2] Garrett C J R. Wave forces on a circular dock[J]. Journal of Fluid Mechanics, 1971, 46(1):129-139.
[3] Yeung R W. Added mass and damping of a vertical cylinder in finite-depth waters[J]. Applied Ocean Research, 1981, 3(3):119-133.
[4] Sabuncu T, Calisal S. Hydrodynamic coefficients for vertical circular cylinders at finite depth[J]. Ocean Engineering, 1981, 8(1):25-63.
[5] Mavrakos S A. Wave loads on a stationary floating bottomless cylindrical body with finite wall thickness[J]. Applied Ocean Research, 1985, 7(4):213-224.
[6] Kokkinowrachos K, Mavrakos S, Asorakos S. Behaviour of vertical bodies of revolution in waves[J]. Ocean Engineering, 1986, 13(6):505-538.
[7] Drobyshevski Y. Hydrodynamic coefficients of a floating, truncated vertical cylinder in shallow water[J]. Ocean Engineering, 2004, 31(3–4):269-304.
[8] Shen Y M, Zheng Y H, You Y G. On the radiation and diffraction of linear water waves by a rectangular structure over a sill. Part I. Infinite domain of finite water depth[J]. Ocean Engineering, 2005, 32(8–9):1073-1097.
[9] Backer G D, Vantorre M, Banasiak R, et al. Numerical modelling of wave energy absorption by a floating point absorber system[J]. 2007:1-2.
[10] Moghadaszadeh S O, Khaji N. Development and application of a semi-analytical method with diagonal coefficient matrices for analysis of wave diffraction around vertical cylinders of arbitrary cross-sections[J]. Ocean Engineering, 2015, 110:292-302.
[11] Filianoti P, Gurnari L, Aristodemo F, et al. Wave flume tests to check a semi-analytical method for calculating solitary wave loads on horizontal cylinders[C]// ASME 2017, International Conference on Ocean, Offshore and Arctic Engineering. 2017:V07AT06A062.
[12] Liu, HX, Ao, JT, Chen, HL, Liu, M, Collu, M, Liu, J. Performance Analysis of a Sea Javelin Wave Energy Converter in Irregular Wave[J]. JOURNAL OF COASTAL RESEARCH, 2018, 83: 932-940
[13] Zheng XB, Zhou SH, Ma Y, Wang LL. Analytical Research on Energy Conversion Characteristic of a Kind of Point Absorber Wave Energy Device[J]. JOURNAL OF COASTAL RESEARCH, 2018, 83: 991-999
[14] Guo W, Zhou YH, Zhang WC, Zhao, QS. Hydrodynamic Analysis and Power Conversion for Point Absorber WEC with Two Degrees of Freedom Using CFD[J]. CHINA OCEAN ENGINEERING, 2018, 38(6):718-729
[15] Lu HC, Tian Z, Zhou L, Liu FS. An improved time-domain response estimation method for floating structures based on rapid solution of a state-space model[J]. OCEAN ENGINEERING, 2019, 173: 628-642
[16] Xu QL, Li Y, Xia YK, Chen WX, Gao F. Performance assessments of the fully submerged sphere and cylinder point absorber wave energy converters[J]. MODERN PHYSICS LETTERS B, 2019, 33(13)
[17] Wang L, Yeung RW. An efficient hybrid integral-equation method for point-absorber wave energy converters with a vertical axis of symmetry[J]. APPLIED OCEAN RESEARCH, 2019, 86: 195-206
[18] Kim SJ, Koo W, Shin, MJ. Numerical and experimental study on a hemispheric point-absorber-type wave energy converter with a hydraulic power take-off system[J]. RENEWABLE ENERGY, 2019, 135: 1260-1269
[19] Budal K, Falnes J. Model experiment with a phase controlled point absorber. Second International Symposium on Wave and Tidal Energy, Cambridge, UK, 1981, 191-206.
[20] Babarit A, Clément A. Optimal latching control of a wave energy device in regular and irregular waves[J]. Applied Ocean Research, 2006, 28(2): 77–91.
[21] Salter SH. Power conversion systems for ducks. International Conference on Future Energy Concepts, January, London, UK, 1979.
[22] Rossiter J A. Model-based predictive control: A practical approach. CRC Press, 2003, Chapter 3.
[23] Brekken T. On model predictive control for a point absorber wave energy converter. IEEE Trondheim Power Technology, Trondheim, Norway, 2011.
[24] Abraham E, Kerrigan E C. Optimal active control and optimization of a wave energy converter. IEEE Transactions on Sustainable Energy, 2013, 4(2): 324-332.
[25] Jin SY, Patton RJ, Guo BY. Enhancement of wave energy absorption efficiency via geometry and power take-off damping tuning[J]. ENERGY, 2019, 169: 819-832
[26] Abdelkhalik O, Zou SY. Control of Wave Energy Converters Using A Simple Dynamic Model[J]. IEEE TRANSACTIONS ON SUSTAINABLE ENERGY, 2019, 10(2), 579-585
[27] Na J, Li G, Wang B, Herrmann G, Zhang SY. Robust Optimal Control of Wave Energy Converters Based on Adaptive Dynamic Programming[J]. IEEE TRANSACTIONS ON SUSTAINABLE ENERGY, 2019, 10(2), 961-970
[28] Zhan SY, Li G, Na J, He W. Feedback noncausal model predictive control of wave energy converters[J]. CONTROL ENGINEERING PRACTICE, 2019, 85, 110-120
[29] Madhi F, Yeung R W, Sinclair M E. ENERGY-CAPTURING FLOATING BREAKWATER:, US20150091304[P]. 2015.Aly A M, Abdelhamid A S, Mahmood A R, et al. A Demonstration of AQWA: Adaptive Query-Workload-Aware Partitioning of Big Spatial Data[C]// PVLDB. 2015:2062-2073.

[30] Zhang WC, Liu HX, Zhang L, Zhang XW. Hydrodynamic analysis and shape optimization for vertical axisymmetric wave energy converters[J]. CHINA OCEAN ENGINEERING, 2016, 30(6), 954-966
[31] Liu M, Liu HX, Zheng XB, Chen HL, Wang LQ, Zhang L. NONLINEAR PTO EFFECT ON PERFORMANCE OF VERTICAL AXISYMMETRIC WAVE ENERGY CONVERTER USING SEMI-ANALYTICAL METHOD[J]. POLISH MARITIME RESEARCH, 2017, 24, 49-57
[32] Chen ZF, Zhou BZ, Zhang L, Sun L, Zhang XW. Performance evaluation of a dual resonance wave-energy convertor in irregular waves[J]. APPLIED OCEAN RESEARCH, 2018, 77, 78-88